Journal of Solid Mechanics Vol. 14, No. 4 (2022) pp. 477-490
DOI: 10.22034/jsm.2021.1933470.1700

Research Paper

The Effect of Magnetic Nanoparticles on Dynamic Behavior of Aorta Artery with Atherosclerosis Under the Action of Pulsating Blood Velocity

M.R. Motaghedifar [1], A. Fakhar [1,*], H. Tabatabaei [1], M. Mazochi [2]

[1]*Department of Mechanical Engineering, Kashan Branch, Islamic Azad University, Kashan, Iran*
[2]*Department of Cardiology, School of Medicine, Kashan University of Medical Sciences, Kashan, Iran*

Received 26 July 2022; accepted 1 October 2022

ABSTRACT

In this article, a biomechanical model is presented for dynamic instability behavior of aorta arteries with atherosclerosis conveying pulsating blood including pharmaceutical nanoparticles. Utilizing Mindlin theory of cylindrical shell, the aorta artery is simulated mathematically. The atherosclerosis is assumed symmetric with lipid tissue. The pharmaceutical nanoparticles are subjected to magnetic field for attract to the lipid tissue in artery. Applying energy method and numerical method of differential quadrature (DQ), the final equations are solved for obtaining the dynamic instability region (DIR). The DIR is curve of dynamic blood velocity with respect to artery frequency. The influences of various variables of magnetic field, magnetic nanoparticle's volume percent, tissue, lipid's height and length upon dynamic behavior of aorta artery are investigated. Based on the results, the existence of magnetic nanoparticle in the blood enhances the artery frequency and consequently can lead to better heart performance and reduce the risk of heart attack.

Keywords : Aorta artery; Atherosclerosis; Pulsating blood flow; Pharmaceutical nanoparticles; Numerical method.

1 INTRODUCTION

PHARMACEUTICAL nanoparticles recently have attract attention among the researchers in medical and biotechnology. For example, the magnetic nanoparticles can be used for drug delivery and relieve the atherosclerosis in the arteries. Hence, in this paper, we focused on the effect of magnetic nanoparticles on dynamic behavior of aorta artery with atherosclerosis. In this regards, Drug delivery based on the pharmaceutical nanoparticles was studied by Bhardwaj et al. [1]. Adibkia et al. [2] reviewed various methods for preparing the pharmaceutical nanoparticles. Hedayatnasab et al. [3] studied hyperthermia cancer therapy on the basis of magnetic nanoparticles. The influence of magnetic nanoparticles on the biomedical was investigated by Mohammed et al. [4].

*Corresponding author.
E-mail address: a.fakhar@iaukashan.ac.ir (A. Fakhar)

Zhou et al. [5] applied a new version of magnetic nanoparticles on Magnetic resonance imaging (MRI). The effect of magnetic nanoparticles on the treat damaged nerves was presented by Raffa [6]. Gloag et al. [7] studied magnetic nanoparticles effects on the novel design and strategies. Thomas et al. [8] presented modified starch alginate nanoparticles utilizing a facile green method in order to drug delivery. The characterization and formation of ISAsomes, mainly hexosomes and cubosomes were studied by Yaghmur and Mu [9]. Maiti et al. [10] investigated the capturing efficiency of nanoparticles with magnetic behaviour for drug delivery into the blood stream. Okeyo et al. [11] studied oral drug delivery on the basis of standard analytical tools and a comprehensive efficacy, stability, and safety was presented. Applications of capillary action which is important choice for drug delivery systems was presented by Li et al. [12]. Cui et al. [13] discussed the ongoing current and clinical completed trials of Nano-drug delivery systems for gliomas therapy. They studied the challenges and trends faced by clinical translation of these well-designed Nano-drug delivery systems. A single peptide–drug conjugate molecule achieves multiple biological functions was presented by Zhu et al. [14]. This was proposed as a novel drug delivery system, the molecular drug delivery system. For the effect of blood flow filed on the arteries, Tubaldi et al. [15] studied dynamic behavior of aortic arteries with assuming various physiological pulsation rates. Ferrari et al. [16] presented an experiment analysis for aortic arteries in order to dynamic response. Buckling of blood vessels was investigate by Sharzehee et al. [17] on the basis of thick walled cylindrical shell element. Liu and Han [18] studied buckling analysis of artery under the pulsatile blood pressure. Vibration and frequency responses of arteries were investigated by Kim et al. [19]. Linget al. [20] studied blood flow in bifurcate channels of arteries on the basis of multiphase Eulerian model. The influences of chemical reaction and heat source on blood flow in bifurcated permeable arteries under the magnetic field were presented by Kumar et al. [21]. Jamil et al. [22] studied the magnetic non-Newtonian Casson blood flow in a stenosed inclined artery. Das et al. [23] studied the rheological perspective of blood flow with the suspension of metallic or non-metallic nanoparticles through arteries. Sarwar and Hussain [24] investigated flow characteristics of human blood under stenoses assumptions. The influence of magnetic field on blood pulsatile flow in a curved stenosed artery was studied by Teimouri et al. [25]. A stenosis growth model was applied by Stamou et al. [26] to study how the flow at the wall change as the stenosis develops.

In this paper, dynamic instability response of aorta arteries with atherosclerosis in tissue matrix including conveying blood with pharmaceutical nanoparticles. For biomechanicsl modeling, the Mindlin theory is utilized and based on energy method, the final governing equations are derived. On the basis of DQ solution method, the DIR of the structure is calculated. The influences of various variables of magnetic field, magnetic nanoparticle's volume percent, tissue, lipid's height and length upon dynamic behavior of aorta artery are investigated.

2 MODELING AORTA ARTERY

Fig. 1(a) depicts an aorta artery having atherosclerosis inserted in human body's tissues and Fig.1(b) illustrates an artery experiences atherosclerosis. Likewise, Fig. 1(c) shows a model of aorta artery biomechanically having atherosclerosis supplying pulsating blood comprising magnetic nanoparticles. As observed, L_{Lipid}, L_b, L_a and R_i respectively express length related to atherosclerosis, length before atherosclerosis, length after atherosclerosis and internal radii. It should be stated that existing tissue encircled artery is simulated through damper as well as spring elements. Using cylindrical coordinate (x, θ, z) in which x, θ and z respectively describe axial, circumferential as well as radial direction, it can be modelled.

(a) (b)

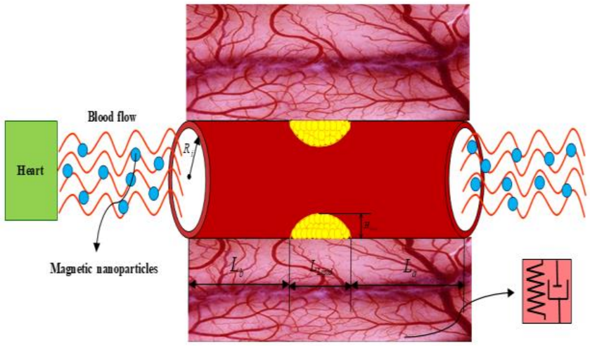

(c)

Fig.1
(a) An aortic artery (b) An artery experiecing atherosclerosis (c) a model of aorta artery biomechanically having atherosclerosis supplying pulsating blood comprising magnetic nanoparticles.

2.1 Strain relations

The displacement field of the aortic artery based on Mindlin theory is [27]

$$u(x,\theta,z,t)=u(x,\theta,t)+z\,\phi_x(x,\theta,t), \tag{1}$$

$$v(x,\theta,z,t)=v(x,\theta,t)+z\,\phi_\theta(x,\theta,t), \tag{2}$$

$$w(x,\theta,z,t)=w(x,\theta,t), \tag{3}$$

where *u, v* and *w* describe mid-plane displacements in the x, θ and z directions; ϕ_x and ϕ_θ are cross section rotations. Furthermore, the strain components are expressed as [27]

$$\varepsilon_{xx}=\frac{\partial u}{\partial x}+z\,\frac{\partial \phi_x}{\partial x}, \tag{4}$$

$$\varepsilon_{\theta\theta}=\frac{1}{R}\left(w+\frac{\partial v}{\partial \theta}\right)+\frac{z}{R}\frac{\partial \phi_\theta}{\partial \theta}, \tag{5}$$

$$\gamma_{x\theta}=\frac{\partial v}{\partial x}+\frac{1}{R}\left(\frac{\partial u}{\partial \theta}\right)+z\left(\frac{\partial \phi_\theta}{\partial x}+\frac{1}{R}\frac{\partial \phi_x}{\partial \theta}\right), \tag{6}$$

$$\gamma_{xz}=\phi_x+\frac{\partial w}{\partial x}, \tag{7}$$

$$\gamma_{z\theta}=\frac{1}{R}\left(\frac{\partial w}{\partial \theta}-v\right)+\phi_\theta, \tag{8}$$

In the mentioned equations, the radii related to artery (R) regarding atherosclerosis is defined as below [28]

$$R(\mathrm{z})=\begin{cases} R_o-\alpha\left[L_{Lipid}^{n-1}\left(z-L_a\right)-\left(z-L_a\right)^n\right] & \textit{In atherosclerosis} \\ R_o & \textit{Before and after atherosclerosis} \end{cases} \tag{9}$$

In which

$$\alpha=\frac{H_{Lipid}\,n^{\frac{n}{n-1}}}{L_{Lipid}^{n}\left(n-1\right)}, \tag{10}$$

where n represents a parameter that can be selected 2.

2.2 Stress relations

The strain (ε_{ij}) –stress (σ_{ij}) relationships are simplified as [27]

$$\begin{bmatrix}\sigma_{xx}\\ \sigma_{\theta\theta}\\ \tau_{xz}\\ \tau_{\theta z}\\ \tau_{x\theta}\end{bmatrix}=\begin{bmatrix}C_{11} & C_{12} & 0 & 0 & 0\\ C_{21} & C_{22} & 0 & 0 & 0\\ 0 & 0 & C_{44} & 0 & 0\\ 0 & 0 & 0 & C_{55} & 0\\ 0 & 0 & 0 & 0 & C_{66}\end{bmatrix}\begin{bmatrix}\varepsilon_{xx}\\ \varepsilon_{\theta\theta}\\ \gamma_{xz}\\ \gamma_{\theta z}\\ \gamma_{x\theta}\end{bmatrix}, \tag{11}$$

where C_{ij} are elastic constants.

2.3 Energy relations

The potential energy (U) of the aorta artery is

$$\begin{aligned}U=&\frac{1}{2}\int_{0}^{2\pi}\int_{0}^{L}\left\{\left[N_{xx}\frac{\partial u}{\partial x}+M_{xx}\frac{\partial\phi_x}{\partial x}\right]+\left[N_{\theta\theta}\frac{\partial v}{R\partial\theta}+M_{\theta\theta}\frac{\partial\phi_\theta}{R\partial\theta}\right]+Q_x\left(\phi_x+\frac{\partial w}{\partial x}\right)+N_{x\theta}\left[\frac{\partial v}{\partial x}+\frac{\partial u}{R\partial\theta}\right]\right.\\ &\left.+M_{x\theta}\left[\frac{\partial\phi_\theta}{\partial x}+\frac{\partial\phi_x}{R\partial\theta}\right]+Q_\theta\left[\frac{\partial w}{R\partial\theta}+\phi_\theta\right]\right\}dA,\end{aligned} \tag{12}$$

where the plane force and moments are

$$\begin{Bmatrix}N_x\\ N_\theta\\ N_{x\theta}\end{Bmatrix}=\int_{-\frac{h}{2}}^{\frac{h}{2}}\begin{Bmatrix}\sigma_x\\ \sigma_\theta\\ \tau_{x\theta}\end{Bmatrix}dz,\quad \begin{Bmatrix}M_x\\ M_\theta\\ M_{x\theta}\end{Bmatrix}=\int_{-\frac{h}{2}}^{\frac{h}{2}}\begin{Bmatrix}\sigma_x\\ \sigma_\theta\\ \tau_{x\theta}\end{Bmatrix}zdz, \tag{13}$$

$$\begin{Bmatrix}Q_x\\ Q_\theta\end{Bmatrix}=k'\int_{-\frac{h}{2}}^{\frac{h}{2}}\begin{Bmatrix}\tau_{x\theta}\\ \tau_{\theta z}\end{Bmatrix}dz, \tag{14}$$

In which k' is shear correction coefficient and h is the thickness of artery. Kinetic energy (K) of the aorta artery is

$$K=\frac{1}{2}\int\begin{pmatrix}I_0\left(\left(\frac{\partial u}{\partial t}\right)^2+\left(\frac{\partial v}{\partial t}\right)^2+\left(\frac{\partial w}{\partial t}\right)^2\right)+I_1\left(2\frac{\partial u}{\partial t}\frac{\partial\phi_x}{\partial t}+2\frac{\partial v}{\partial t}\frac{\partial\phi_\theta}{\partial t}\right)\\ +I_2\left(\left(\frac{\partial\phi_x}{\partial t}\right)^2+\left(\frac{\partial\phi_\theta}{\partial t}\right)^2\right)\end{pmatrix}dA. \tag{15}$$

where ρ is the aorta artery density and the moments of inertia are

$$\begin{Bmatrix} I_0 \\ I_1 \\ I_2 \end{Bmatrix} = \int_{-h/2}^{h/2} \begin{bmatrix} \rho \\ \rho z \\ \rho z^2 \end{bmatrix} dz \,. \tag{16}$$

It should be noticed that the external work contain four section including work of blood flow, work of tissue covering artery, works related to magnetic load and nanoparticle drag.

Work of tissue. In order to model the tissues and muscles around the artery, viscoelastic model is utilized with damping constants, C_d , and spring constants, k_w . Hence, the work of tissues according to viscoelastic model is [27]

$$q_{tissue} = -k_w w - C_d \dot{w} \,, \tag{17}$$

Work of blood flow. The flow of blood in the aorta artery is assumed pulsating, axially symmetric and laminar. The widely known Navier-Stokes equation is expressed as below [28]

$$\rho_e \frac{d\mathrm{V}}{dt} = -\nabla \mathrm{P} + \mu_e \nabla^2 \mathrm{V} + \mathrm{F}_{body} \,, \tag{18}$$

In which **P**, μ_e and ρ_e respectively represent the blood's pressure, the blood's viscosity and the blood's density and F_{body} expresses the body forces. Likewise, based on Navier-Stokes equation, total derivative operator according to t is [28]

$$\frac{d}{dt} = \frac{\partial}{\partial t} + v_x \frac{\partial}{\partial x} + v_\theta \frac{\partial}{\partial \theta} + v_z \frac{\partial}{\partial z} \,, \tag{19}$$

In the contact point of fluid and artery, the relative velocity as well as acceleration in radial direction are considered equal. Therefore,

$$v_z = \frac{dw}{dt} \,, \tag{20}$$

Substituting Eqs. (19) and (20) into Eq. (18), the induced pressure by blood flow can be written as:

$$\frac{\partial p_z}{\partial z} = -\rho_e \left(\frac{\partial^2 w}{\partial t^2} + 2v_x \frac{\partial^2 w}{\partial x \, \partial t} + v_x^{\,2} \frac{\partial^2 w}{\partial x^2} \right) + \mu_e \left(\frac{\partial^3 w}{\partial x^2 \, \partial t} + \frac{\partial^3 w}{R^2 \, \partial \theta^2 \, \partial t} + v_x \left(\frac{\partial^3 w}{\partial x^3} + \frac{\partial^3 w}{R^2 \, \partial \theta^2 \, \partial x} \right) \right), \tag{21}$$

Mmultiplying the whole Eq. (21) by the inside artery area, A, the radial force with respect to pulsation of blood flow, $v_x = V0 + V0\cos(\omega \mathrm{t})$ where V_0 is the constant blood velocity and ω is the pulsation frequency, in artery is counted as below

$$q_{fluid} = A \frac{\partial p_z}{\partial z} = -\rho_e \left(\frac{\partial^2 w}{\partial t^2} + 2v_x \frac{\partial^2 w}{\partial x \, \partial t} + v_x^{\,2} \frac{\partial^2 w}{\partial x^2} \right) + \mu_e \left(\frac{\partial^3 w}{\partial x^2 \, \partial t} + \frac{\partial^3 w}{R^2 \, \partial \theta^2 \, \partial t} + v_x \left(\frac{\partial^3 w}{\partial x^3} + \frac{\partial^3 w}{R^2 \, \partial \theta^2 \, \partial x} \right) \right), \tag{22}$$

In the mentioned equations, the blood's density as well as viscosity conveying magnetic nanoparticles are expressed as [29]

$$\rho_e = (1-\phi)\rho_f + \phi \rho_p \,, \tag{23}$$

$$\mu_e = \left(1 + 39.11\phi + 533.9\phi^2\right)\mu_f \,, \tag{24}$$

In which ϕ indicates volume percent of nanoparticles and the subscripts p and f respectively refer to nanoparticles as well as fluid.

Computation of magnetic force. For the a particle of volume *V*, the magnetization force, $\mathbf{F}_m$, which is recognized as Kelvin force can be expressed as [29]

$$\mathbf{F}_m = \iiint_V \mu_0 \mathbf{M} \times \nabla \mathbf{H} dV \tag{25}$$

In which μ_0 refers to nanoparticle's magnetic permeability and its amount is $4\pi \times 10^{-7}$ $\left(\mathrm{NA}^{-2}\right)$. Further, $\mathbf{M}$ describes magnetization of materials and $\mathbf{H}$ indicates magnetic field. Moreover, over defined magnetic field, the magnetization saturates to permanent amount M_{sat} which causes the model written below [29]

$$\mathbf{M} = \begin{cases} \chi_{eff}\,\mathbf{H} & H < M_{sat}/\chi_{eff} \\ M_{sat}\,\hat{\mathbf{H}} & H \geq M_{sat}/\chi_{eff} \end{cases} \tag{26}$$

It should be noted that effective vulnerability of spherical particles is relevant to their innate vulnerability χ_{eff} as $\chi_{eff} = \left[\chi_i/(1+1/3\chi_i)\right]$. In this state, a hat is utilized in order to show unit vector, $\hat{\mathbf{H}} = \mathbf{H}/H$, where $H = |\mathbf{H}|$. Moreover, the mentioned relation for curl free magnetic field can be given by [28, 29]

$$\mathbf{F}_m = \begin{cases} \dfrac{\pi d_p^3}{6}\mu_0 \dfrac{\chi_{eff}}{2}\nabla \mathrm{H}^2 & H < M_{sat}/\chi_{eff} \\ \dfrac{\pi d_p^3}{6}\mu_0 M_{sat}\nabla \mathrm{H} & H \geq M_{sat}/\chi_{eff} \end{cases} \tag{27}$$

Work of nanoparticle drag. The drag force for every particle volume can be given by [28]

$$F_D = \frac{18\mu C_D \,\mathrm{Re}}{24\rho_p d_p^2} \tag{28}$$

where is the μ viscousity, *Re* is the Reynoldz number, ρ_p is the density of nanoparticles and d_p is the nanoparticles diameter. Furthermore, drag constant, C_D, in the conditions that the particles are smooth, the spherical drag are written as:

$$C_D = a_1 + \frac{a_2}{\mathrm{Re}} + \frac{a_3}{\mathrm{Re}^2} \tag{29}$$

In which a_1, a_2 and a_3 represent the coefficients which use over various amounts of *Re* [29].

2.4 Motion equations

Now, applying Hamilton's principle, we have the following motion equations

$$\delta u: \frac{\partial N_{xx}}{\partial x} + \frac{\partial N_{x\theta}}{R\,\partial\theta} = I_0 \frac{\partial^2 u}{\partial t^2} + I_1 \frac{\partial^2 \phi_x}{\partial t^2}, \tag{30}$$

$$\delta v\ :\frac{\partial N_{x\theta}}{\partial x}+\frac{\partial N_{\theta\theta}}{R\,\partial\theta}=I_0\frac{\partial^2 v}{\partial t^2}+I_1\frac{\partial^2\phi_\theta}{\partial t^2}, \tag{31}$$

$$\delta w\ :\frac{\partial Q_x}{\partial x}+\frac{\partial Q_\theta}{R\,\partial\theta}-q_{tissue}-q_{fluid}-F_M-F_D=I_0\frac{\partial^2 w}{\partial t^2}, \tag{32}$$

$$\delta\phi_x\ :\frac{\partial M_{xx}}{\partial x}+\frac{\partial M_{x\theta}}{R\,\partial\theta}-Q_x=I_2\frac{\partial^2\phi_x}{\partial t^2}+I_1\frac{\partial^2 u}{\partial t^2}, \tag{33}$$

$$\delta\phi_\theta :\frac{\partial M_{x\theta}}{\partial x}+\frac{\partial M_{xx}}{R\,\partial\theta}-Q_\theta=I_2\frac{\partial^2\phi_\theta}{\partial t^2}+I_1\frac{\partial^2 v}{\partial t^2}. \tag{34}$$

Substituting stress-strain relations from Hook's law into Eqs. (12)-(14), the stress resultant-displacement relations can be obtained as follow:

$$N_{xx}=A_{110}\frac{\partial u}{\partial x}+A_{111}\frac{\partial\phi_x}{\partial x}+A_{120}\frac{\partial v}{\partial y}+A_{121}\frac{\partial\phi_\theta}{R\,\partial\theta}, \tag{35}$$

$$N_{\theta\theta}=A_{120}\frac{\partial u}{\partial x}+A_{121}\frac{\partial\phi_x}{\partial x}+A_{220}\frac{\partial v}{\partial y}+A_{221}\frac{\partial\phi_\theta}{R\,\partial\theta}, \tag{36}$$

$$Q_\theta=k^{'}A_{44}\left[\frac{\partial w}{R\,\partial\theta}+\phi_\theta\right], \tag{37}$$

$$Q_x=k^{'}A_{55}\left(\frac{\partial w}{\partial x}+\phi_x\right), \tag{38}$$

$$N_{x\theta}=A_{660}\left(\frac{\partial u}{\partial y}+\frac{\partial v}{\partial x}\right)+A_{661}\left(\frac{\partial\phi_x}{R\,\partial\theta}+\frac{\partial\phi_\theta}{\partial x}\right), \tag{39}$$

$$M_{xx}=A_{111}\frac{\partial u}{\partial x}+A_{112}\frac{\partial\phi_x}{\partial x}+A_{121}\frac{\partial v}{R\,\partial\theta}+A_{122}\frac{\partial\phi_\theta}{R\,\partial\theta}, \tag{40}$$

$$M_{\theta\theta}=A_{121}\frac{\partial u}{\partial x}+A_{122}\frac{\partial\phi_x}{\partial x}+A_{221}\frac{\partial v}{R\,\partial\theta}+A_{222}\frac{\partial\phi_\theta}{R\,\partial\theta}, \tag{41}$$

$$M_{x\theta}=A_{661}\left(\frac{\partial u}{R\,\partial\theta}+\frac{\partial v}{\partial x}\right)+A_{662}\left(\frac{\partial\phi_x}{R\,\partial\theta}+\frac{\partial\phi_\theta}{\partial x}\right), \tag{42}$$

where

$$A_{11k}=\int_{-h/2}^{h/2}C_{11}z^k dz\,,\qquad k=0,1,2 \tag{43}$$

$$A_{12k}=\int_{-h/2}^{h/2}C_{12}z^k dz\qquad k=0,1,2 \tag{44}$$

$$A_{22k}=\int_{-h/2}^{h/2}C_{22}z^k dz\,,\qquad k=0,1,2 \tag{45}$$

$$A_{66k}=\int_{-h/2}^{h/2}C_{66}z^{k}dz\,,\qquad\qquad k=0,1,2 \tag{46}$$

$$A_{44}=\int_{-h/2}^{h/2}C_{44}dz\,, \tag{47}$$

$$A_{55}=\int_{-h/2}^{h/2}C_{55}dz\,. \tag{48}$$

Substituting Eqs. (35)-(42) into Eqs. (30)-(34) yields the motion equations in terms of displacements.

3 SOLUTION PROCEDURE

There is a lot of numerical method to solve the initial-and/or boundary value problems which occur in engineering domain. Some of the common numerical methods are finite element method (FEM), Galerkin method, finite difference method, DQM and etc. FEM and FD method for higher-order modes require to a great number of grid points. Therefore these solution methods for all these points need to more CPU time, while the DQM has several benefits that are listed as below [30-32]:

1. GDQM is a powerful method which can be used to solve numerical problems in the analysis of structural and dynamical systems.
2. The accuracy and convergence of the GDQM is higher than FEM.
3. GDQM is an accurate method for solution of nonlinear differential equations in approximation of the derivatives.
4. This method can easily and exactly satisfy a variety of boundary conditions and require much less formulation and programming effort.
5. Recently, GDQM has been extended to handle irregular shaped.

Due to the above striking merits of the GDQM, in recent years the method has become increasingly popular in the numerical solution of problems in engineering and physical science. Utilizing DQM, the governing equations can be solved numerically. In this method, the differential equations of cylindrical shell can be converted to set of algebraic equations using following relations [30-32]

$$\frac{d^{n}F(x_i,\theta_j)}{dx^{n}}=\sum_{k=1}^{N_x}A_{ik}^{(n)}F(x_k,\theta_j)\qquad\qquad n=1,...,N_x-1, \tag{49}$$

$$\frac{d^{m}F(x_i,\theta_j)}{d\theta^{m}}=\sum_{l=1}^{N_\theta}B_{jl}^{(m)}F(x_i,\theta_l)\qquad\qquad m=1,...,N_\theta-1, \tag{50}$$

$$\frac{d^{n+m}F(x_i,\theta_j)}{dx^{n}d\theta^{m}}=\sum_{k=1}^{N_x}\sum_{l=1}^{N_\theta}A_{ik}^{(n)}B_{jl}^{(m)}F(x_k,\theta_l), \tag{51}$$

In which the weighting coefficients ($A_{ik}^{(n)}$ and $B_{jl}^{(m)}$) are expressed as:

$$A_{ij}^{(1)}=\begin{cases}\dfrac{\prod\limits_{\substack{j=1\\ j\neq i}}^{N_x}(x_i-x_j)}{(x_i-x_j)\prod\limits_{\substack{j=1\\ j\neq i}}^{N_x}(x_i-x_j)}, & for\quad i\neq j,\quad i,j=1,2,...,N_x\\ -\sum\limits_{\substack{j=1\\ i\neq j}}^{N_x}A_{ij}^{(1)}, & for\quad i=j,\quad i,j=1,2,...,N_x\end{cases} \tag{52}$$

$$B_{ij}^{(1)} = \begin{cases} \dfrac{\prod_{\substack{j=1\\ j\neq i}}^{N_\theta}(\theta_i-\theta_j)}{(\theta_i-\theta_j)\prod_{\substack{j=1\\ j\neq i}}^{N_\theta}(\theta_i-\theta_j)}, & for \quad i\neq j, \quad i,j=1,2,...,N_\theta, \\ -\sum_{\substack{j=1\\ i\neq j}}^{N_\theta} B_{ij}^{(1)}, & for \quad i=j, \quad i,j=1,2,...,N_\theta \end{cases} \tag{53}$$

In addition, the number of grid points in x and θ directions can be written based on Chebyshev polynomials as:

$$x_i = \frac{L}{2}\left[1-\cos\left(\frac{i-1}{N_x-1}\right)\pi\right], \qquad i=1,...,N_x \tag{54}$$

$$\theta_i = \frac{2\pi}{2}\left[1-\cos\left(\frac{i-1}{N_\theta-1}\right)\pi\right]. \qquad i=1,...,N_\theta \tag{55}$$

Finally, utilizing DQM, the governing equations in matrix form can be expressed as:

$$\begin{aligned} &[M]_{5N_xN_\theta\times 5N_xN_\theta}\{\ddot{d}\}_{5N_xN_\theta\times 1}+\left([C]_{5N_xN_\theta\times 5N_xN_\theta}+(V_0+V_0\alpha\cos(\omega t))[C]^f{}_{5N_xN_\theta\times 5N_xN_\theta}\right)\{\dot{d}_{5N_xN_\theta\times 1}\} \\ &+\left([K]_{5N_xN_\theta\times 5N_xN_\theta}+(V_0+V_0\alpha\cos(\omega t))^2[K]^f{}_{5N_xN_\theta\times 5N_xN_\theta}\right)\{d_{5N_xN_\theta\times 1}\}=0, \end{aligned} \tag{56}$$

In which $[M]$, $[C]$ and $[K]$ respectively describe mass matrix, damping matrix and stiffness matrix. Further, $[K]^f$ and $[C]^f$ respectively represent stiffness matrix as well as damping matrix for pulsating fluid and $\{d\}=\{u,v,w,\phi_x,\phi_\theta\}$ defines dynamic displacement vector. Noted that the dimension of matrices are $5N_xN_\theta\times 5N_xN_\theta$ and the order of dynamic vector is $5N_xN_\theta\times 1$.

3.1 Bolotin method

According to Bolotin's procedure, constituents of $\{d\}$ are defined in Fourier series having period $2T$ as [33]

$$\{d\} = \sum_{k=1,3,...}^{\infty}\left[\{a\}_k\sin\frac{\omega t}{2}+\{b\}_k\cos\frac{\omega t}{2}\right], \tag{57}$$

Substituting Eq. (57) into Eq. (56) and considering the terms of coefficients of cosine and sine, plus sum of the constant as zero, yields

$$\left|\left([K]+\left(1\pm\alpha+\frac{\alpha^2}{2}\right)[K]^f\right)+\left(\pm[C]\frac{\omega}{2}+\left(\frac{\alpha\omega}{4}\pm\frac{\omega}{2}\right)[C]^f\right)-[M]\frac{\omega^2}{4}\right|=0, \tag{58}$$

For obtaining the variation of ω as well as dynamic instability region according to β, above equation is solved with respect to the eigenvalue problem as:

$$\begin{bmatrix} [0] & [I] \\ -\frac{1}{4}[M]^{-1}\left([K]+\left(1\pm\alpha+\frac{\alpha^2}{2}\right)[K]^f\right) & \frac{1}{4}[M]^{-1}\left(\pm[C]\frac{\omega}{2}+\left(\frac{\alpha\omega}{4}\pm\frac{\omega}{2}\right)[C]^f\right)\end{bmatrix}\begin{bmatrix}[d]\\ [\dot{d}]\end{bmatrix}=\begin{bmatrix}[0]\\ [0]\end{bmatrix}. \tag{59}$$

The above relation can be solved by eigenvaluen technique.

4 DISCUSSION AND NUMERICAL CONSEQUENCES

For parametric study, an aorta artery is assumed with inner radii, $R_1 = 3.38\ mm$, outer radii, $R_2 = 5.38\ mm$, length, $L = 45\ mm$, thickness and $h = 1\ mm$ [34]. Based on Ref. [35], the velocity range of blood is considered and according to Ref. [36], the frequency of heart pulse for humans is selected 2 Hz. The Mechanical properties of artery are listed in Table 1.

Table 1
Mechanical properties of artery. [34]

Parameter	Value	Unit
Young's modulus	130	*KPa*
Poisson's ratio	0.3	---
Density of artery	1300	Kg/m^3
Density of blood	1056	Kg/m^3
Density of nanoparticles	1800	Kg/m^3

4.1 Validation

In order to validate the results of this paper, the magnetic nanoparticles and blood flow are neglected and buckling of arteries is studied. As shown in Table 2, the critical bucking pressure for various arteries is reported and it is obvious that the obtained results are in a good accordance with Ref. [37]

Table 2
Comparison of present work with critical buckling pressure in Ref. [37]

Vessel	Experimental	Present work
L=45 *mm*, *h*=1 *mm*	44	43.81
L =44 *mm*, *h* =0.5 *mm*	50.5	50.22
L =52.2 *mm*, *h* =1.46 *mm*	60	60.12
L =47.2 *mm*, *h* =1.55 *mm*	55	54.91

4.2 Solution method convergence

Fig. 2 shows the DIR of the aorta artery for different grid point numbers. It is found that with enhancing the grid point numbers, the resonance frequency is decreased and consequently, in *N*=17, the results will be converged.

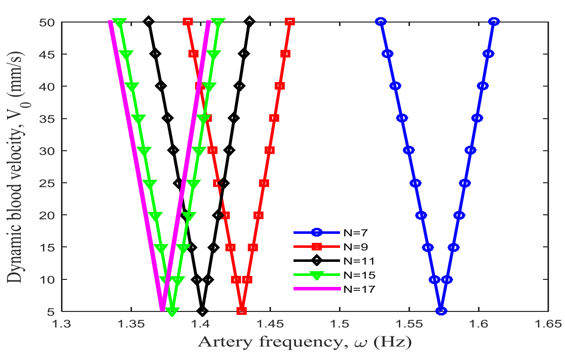

Fig.2
Influence of various DQM grid points number on DIR of aorta artery with atherosclerosis.

4.3 Parametric study

In all of the figures, the pulsation frequency is evaluated versus velocity of dynamic fluid. Hence, the instable regions which are inside the boundary curve and stable regions which are outside the boundary curve are shown. Fig. 3 presents the magnetic nanoparticle volume percent effects on the DIR of the aorta artery. It is obvious that increment of magnetic nanoparticle volume percent result in move of DIR to the right and enhances of excitation frequency. In fact, presence of such materials in the blood can lead to better heart performance and consequently reduce the risk of heart attack.

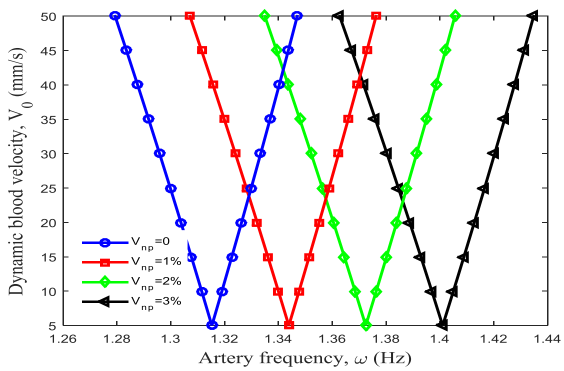

Fig.3
Influence of magnetic nanoparticle volume percent on DIR of aorta artery.

The magnetic nanoparticle diameter influence upon DIR of aorta artery is illustrated in Fig. 4. It is vivid that rise of magnetic nanoparticle diameter in blood causes decrease in pulsation frequencies of aorta artery. It is since with enhancing the magnetic nanoparticle diameter, the thermo-physical characteristics of nanoparticle is reduced.

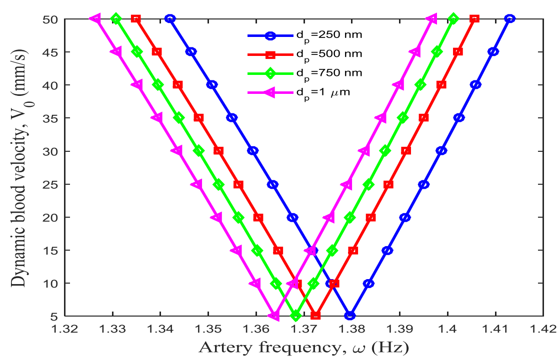

Fig.4
Influence of magnetic nanoparticle diameter on DIR of aorta artery.

The effects of lipid tissue's length and height on the DIR of an aortic artery respectively are presented in Fig. 5 and 6, respectively. It is found that with enhancing the height and length of lipid tissue leads to lower frequency and hence the DIR shifts to left. It is physically true since with enhancing the lipid tissue's length and height, the stiffness of the artery decreases.

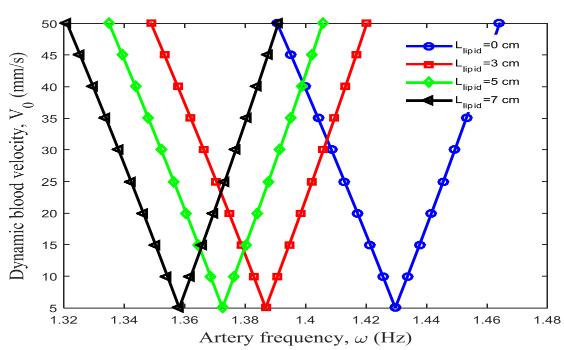

Fig.5
Influence of lipid tissue's length on DIR of aorta artery.

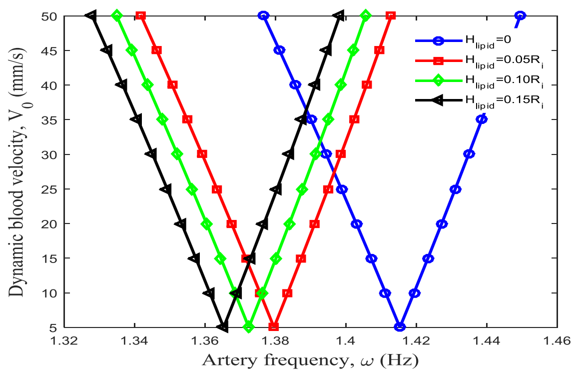

Fig.6
Influence of lipid tissue's height on DIR of aorta artery.

Fig. 7 presents the DIR of the aorta artery for various magnetic fields. It is vivid that by enhancing the magnetic field, the DIR moves to higher frequencies. In other words, with enhancing the magnetic field, the stiffness of the artery is increased. Therefore, utilizing magnetic field leads to attack of pharmaceutical nanoparticles to lipid tissue and consequently can amend artery's performance and diminish heart attacks.

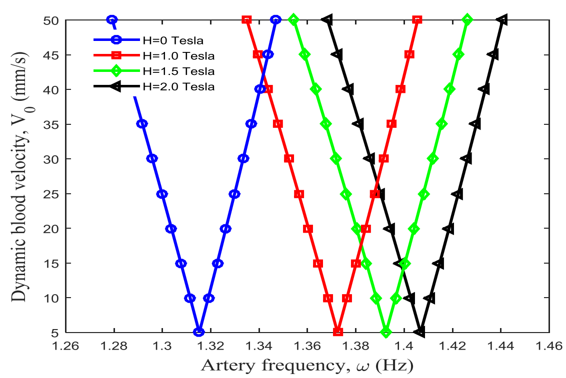

Fig.7
Influence of magnetic fields on DIR of aorta artery.

Fig. 8 shows the tissue effect on the DIR of aorta artery. As can be found, with strong mussels, the DIR shift to the higher amounts of pulsation frequencies of aorta artery. Hence, by reinforcing tissue using various method including sport, the percentage of tortuosity as well as failure causing transitory ischemic attacks, diabetes, aging, infract and cardiovascular diseases can be reduced [30].

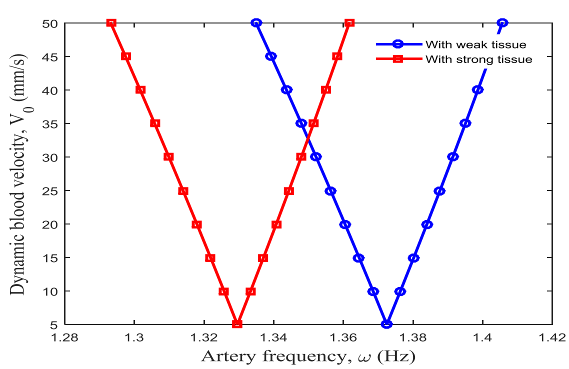

Fig.8
Influence of tissue around the aorta artery on DIR.

5 CONCLUSION

Presenting a biomechanical model for dynamic stability of aorta arteries conveying blood including magnetic nanoparticles with atherosclerosis was the main contribution of this work. The surrounding tissue is modelled by viscoelastic model. Exerting magnetic field results in attraction of lipid tissue in artery by magnetic nanoparticles drug carriers. On the basis of Hamilton's principle, the DIR of aorta artery was calculated utilizing DQ and Bolotin methods. The influences of magnetic field, lipid's height and length, magnetic nanoparticle's volume percent and surrounded tissue upon DIR of aorta artery were analyzed. The results show that increment of both length and height of aorta artery leads to rise of pulsating frequencies. In addition, utilizing magnetic field leads to attack of pharmaceutical nanoparticles to lipid tissue and consequently can amend artery's performance and diminish heart attacks. Furthermore, . It is obvious that increment of magnetic nanoparticle volume percent result in move of DIR to the right and enhances of excitation frequency.

REFERENCES

[1] Bhardwaj V., Hariharan S., Balasubramanian I., Lamprecht A., 2005, Pharmaceutical aspects of polymeric nanoparticles for oral drug delivery, *Journal of Biomedical Nanotechnology* **1**: 235-258.

[2] Adibkia K., Nokhodchi A., Siah-Shadbad M., Omidi Y., Javadzadeh Y., Mohammadi G., 2009, A review on the methods of preparation of pharmaceutical nanoparticles, Journal Pharmaceutical Sciences **15**: 303-314.

[3] Hedayatnasab Z., Abnisa F., Daud W., 2017, Review on magnetic nanoparticles for magnetic nanofluid hyperthermia application, *Materials and Design* **123**: 174-196.

[4] Mohammed L., Gomaa H. G., Ragab D., Zhu J., 2017, Magnetic nanoparticles for environmental and biomedical applications: A review, *Particuology* **30**: 1-14.

[5] Zhou Z., Yang L., Gao J., Chen X., 2019, Structure–relaxivity relationships of magnetic nanoparticles for magnetic resonance imaging, *Advanced Materials* **31**: 1804567.

[6] Raffa V., 2020, Engineering magnetic nanoparticles for repairing nerve injuries, *Advances in Nanostructured Materials and Nanopatterning Technologies* **2020**: 167-200.

[7] Gloag L., Mehdipour M., Chen D., Tilley R. D., Gooding J. J., 2020, Advances in the application of magnetic nanoparticles for sensing, *Advanced Materials* **31**: 1904385.

[8] Thomas D., Mathew N., Nath Megha S., 2021, Starch modified alginate nanoparticles for drug delivery application, *International Journal of Biological Macromolecules* **173**: 277-284.

[9] Yaghmur A., Mu H., 2021, Recent advances in drug delivery applications of cubosomes, hexosomes, and solid lipid nanoparticles, *Acta Pharmaceutica Sinica B* **11**: 871-885.

[10] Maiti S., Shaw S., Shit G. C., 2021, Fractional order model of thermo-solutal and magnetic nanoparticles transport for drug delivery applications, *Colloids and Surfaces B: Biointerfaces* **203**: 111754.

[11] Okeyo P.O., Rajendran S.T., Boisen A., 2021, Sensing technologies and experimental platforms for the characterization of advanced oral drug delivery systems, *Advanced Drug Delivery Reviews* **176**: 113850.

[12] Li X., Zhao Y., Zhao C., 2021, Applications of capillary action in drug delivery, *IScience* **24**: 102810.

[13] Cui J., Xu Y., Tu H., Zhou H., Wang H., Di L., Wang R., 2021, Gather wisdom to overcome barriers: Well-designed nano-drug delivery systems for treating gliomas, *Acta Pharmaceutica Sinica B* **12**: 1100-1125.

[14] Zhu Y.Sh., Tang K., Lv J., 2021, Peptide–drug conjugate-based novel molecular drug delivery system in cancer, *Trends in Pharmacological Sciences* **42**: 857-869.

[15] Tubaldi E., Ferrari G., Balasubramanian P., Amabili M., 2019, Dynamic behavior of a Dacron aortic graft, *ASME 2019 International Mechanical Engineering Congress and Exposition*.

[16] Ferrari G., Balasubramanian P., Tubaldi E., Giovanniello F., Amabili M., 2019, Experiments on dynamic behavior of a Dacron aortic graft in a mock circulatory loop, *Journal of Biomechanics* **86**: 132-140.

[17] Sharzehee M., Fatemifar F., Han H-C., 2019, Computational simulations of the helical buckling behavior of blood vessels, *Numerical Methods in Biomedical Engineering* **35**: 3277.

[18] Liu Q., Han H-C., 2012, Mechanical buckling of artery under pulsatile pressure, *Journal of Biomechanics* **45**: 1192-1198.

[19] Kim E., Okamoto T., Song J., Lee K., 2020, The acute effects of different frequencies of whole-body vibration on arterial stiffness, *Clinical and Experimental Hypertension* **42**: 345-351.

[20] Ling Y., Tang J., Liu H., 2021, Numerical investigation of two-phase non-Newtonian blood flow in bifurcate pulmonary arteries with a flow resistant using Eulerian multiphase model, *Chemical Engineering Science* **233**: 116426.

[21] Kumar D., Satyanarayana B., Deo N., 2021, Application of heat source and chemical reaction in MHD blood flow through permeable bifurcated arteries with inclined magnetic field in tumor treatments, *Results in Applied Mathematics* **10**: 100151.

[22] Fatin Jamil D., Saleem S., Ud Din S., 2021, Analysis of non-Newtonian magnetic Casson blood flow in an inclined stenosed artery using Caputo-Fabrizio fractional derivatives, *Computer Methods and Programs in Biomedicine* **203**: 106044.

[23] Das S., Pal T. K., Janan R.N., Giri B., 2021, Significance of Hall currents on hybrid nano-blood flow through an inclined artery having mild stenosis: Homotopy perturbation approach, *Microvascular Research* **137**:104192.

[24] Sarwar L., Hussain A., 2021, Flow characteristics of Au-blood nanofluid in stenotic artery, *International Communications in Heat and Mass Transfer* **127**: 105486.

[25] Teimouri K., Tavakoli M.R., Kim K.Ch., 2021, Investigation of the plaque morphology effect on changes of pulsatile blood flow in a stenosed curved artery induced by an external magnetic field, *Computers in Biology and Medicine* **135**: 104600.

[26] Stamou A.C., Radulovic J., Buick J.M., 2021, Effect of stenosis growth on blood flow at the bifurcation ofthe carotid artery, *Journal of Computational Science* **54**: 101435.

[27] Reddy J. N., 2004, *Mechanics of Laminated Composite Plates and Shells*, Washington, CRC press.

[28] Bose S., Banerjee M., 2015, Effect of non-Newtonian characteristics of blood on magnetic particle capture in occluded blood vessel, *Journal of Magnetism and Magnetic Materials* **374**: 611-623.

[29] Reddy J. N., Wang C. M., 2004, *Dynamics of Fluid-Conveying Beams: Governing Equations and Finite Element Models*, Singapore: Centre for Offshore Research and Engineering.

[30] Johnston M., Johnston P.R., Corney S., Kilpatrick D., 2004, Non-Newtonian blood flow in human right coronary arteries: steady state simulations, *Journal of Biomechanics* **37**: 709-720.

[31] Civalek Ö., 2004, Application of differential quadrature (DQ) and harmonic differential quadrature (HDQ) for buckling analysis of thin isotropic plates and elastic columns. *Engineering Structures* **26**: 171-186.

[32] Chen W., 1996, *Differential Quadrature Method and its Applications in Engineering*, Department of Mechanical Engineering, Shanghai Jiao Tong University.

[33] Shu C., 1999, *Differential Quadrature and its Application in Engineering*, Springer.

[34] Bolotin V.V., 1964, *The Dynamic Stability of Elastic Systems*, Holden-Day, San Francisco.

[35] Liu Q., Han H.C., 2012, Mechanical buckling of artery under pulsatile pressure, *Journal of Biomechanics* **45**: 1192-1198.

[36] Jozwik K., Obidowski D., 2010, Numerical simulations of the blood flow through vertebral arteries, *Journal of Biomechanics* **43**: 177-185.

[37] Han H.C., 2008, Nonlinear buckling of blood vessels: A theoretical study, *Journal of Biomechanics* **41**: 2708-2713.